Polymer 49 (2008) 2886–2897

Contents lists available at ScienceDirect

Polymer

journal homepage: www.elsevier.com/locate/polymer

Solid-state NMR characterization of unsaturated polyester thermoset blends containing PEO–PPO–PEO block copolymers

Xinjuan Li [a], Weigui Fu [b], Yinong Wang [a], Tiehong Chen [a], Xiaohang Liu [a], Hai Lin [a], Pingchuan Sun [a,*], Qinghua Jin [b], Datong Ding [b]

[a] Key Laboratory of Functional Polymer Materials, Ministry of Education, College of Chemistry, Nankai University, Weijin Road 94, Tianjin 300071, China
[b] College of Physics, Nankai University, Weijin Road 94, Tianjin 300071, China

ARTICLE INFO

Article history:
Received 7 November 2007
Received in revised form 4 April 2008
Accepted 21 April 2008
Available online 26 April 2008

Keywords:
Solid-state NMR
Interphase
Thermoset blends

ABSTRACT

First, the NMR method proposed in our previous work was improved to provide more accurate measurement of interphase thickness in multiphase polymers. Then the improved method, in combination with other techniques, was applied to elucidate the phase behavior, miscibility, heterogeneous dynamics and microdomain structure in thermoset blends of unsaturated polyester resin (UPR) and amphiphilic poly(ethylene oxide)-*block*-poly(propylene oxide)-*block*-poly(ethylene oxide) (PEO–PPO–PEO) triblock copolymer. The experimental results were compared with those of epoxy resin (ER)/PEO–PPO–PEO blends to systematically elucidate the influence of binary polymer–polymer interaction on the phase behavior, domain size and especially the interphase thickness in thermoset blends of UPR and ER, respectively, with the same PEO–PPO–PEO triblock copolymer. It was found that UPR/PEO–PPO–PEO exhibits strong phase separation with considerably small interphase, and only a small fraction of PEO is mixed with UPR. Whereas ER/PEO–PPO–PEO exhibits weak phase separation with thick interphase, and a large amount of PEO is intimately mixed with ER. It was suggested that the thermodynamic interaction between the block copolymer and cross-linked thermoset resin is one of the key factors in controlling the phase behavior, domain size and interphase thickness in these blends. These NMR results are qualitatively in good agreement with the previous theoretical prediction of interphase properties between two immiscible polymers. Our NMR works on different thermoset blend systems with weak and strong microphase separations clearly demonstrate that the improved NMR method is a general and useful method for measuring the interphase thickness and elucidating the phase behavior and subtle microdomain structure in multiphase polymers with detectable heterogeneous dynamics.

1. Introduction

Polymer blends by blending of different components with different properties have been widely employed to produce high performance polymeric materials in the past decades [1,2]. Since the motivating work of Bates and co-workers in 1997 [3,4], toughening of the thermosetting resin by blending with self-assembled amphiphilic block copolymers [5] has received considerable attention due to the unique nanostructured morphologies, physical properties and potential industrial applications of the blends [6–13]. Understanding the factors controlling phase separation and the microdomain structure is crucial for tailoring the nanostructure and developing advanced thermoset resin/block copolymer blends with desired physical and chemical properties [12], and also can shed light on the fundamental issues in phase separation theory for these novel polymerization-induced [1,14,15] and self-assembled thermoset blends. In thermoset resin/block copolymer blends, the final structure and morphologies are determined by several factors including the cross-linking reaction of the thermosetting resin, the self-assembly of the block copolymers and the phase separation of the blend [6–11]. By varying the volume fraction of one block or the chemical structure of the block copolymer, different nanostructures and morphologies in thermoset blends have been observed [6–13]. It is also expected that the thermodynamic interaction between the block copolymer and cross-linked thermoset resin is another important factor controlling the phase behavior and microdomain structure of the blends. By varying the binary component interaction, the mechanism of phase separation in these novel thermoset blends can be well elucidated. Blending of PEO-containing amphiphilic block

* Corresponding author. Tel.: +86 22 23508171; fax: +86 22 23494422.
E-mail address: spclbh@nankai.edu.cn (P. Sun).

0032-3861/$ – see front matter © 2008 Elsevier Ltd. All rights reserved.
doi:10.1016/j.polymer.2008.04.042

copolymers with epoxy resin (ER) have been widely employed to prepare nanostructured thermosetting blends by several groups [6–13,16]. Unsaturated polyester resin (UPR) is another important thermosetting polymer and has been widely used in industrial field. However, only few works were reported on preparing nanostructured blends of unsaturated polyester resin with block copolymers [17–20]. It is expected that the different binary component interactions in blends of UPR and ER, respectively, with the same block copolymer should result in distinct phase behavior, miscibility and microdomain structure.

The knowledge of interphase properties is crucial for understanding the phase behavior and structure–property relationship in multiphase polymers, and studies in this field have attracted significant attention in the past decades. On the basis of the self-consistent mean-field theory, Helfand and co-workers predicted a quantitative relationship between interphase thickness and the thermodynamic interaction parameter χ [21–23]. On the other hand, experimentally quantitative determination of the nanoscale interphase properties, such as interphase thickness and the chemical composition in the interphase region, is still a challenge due to the extremely small volume fraction of interphase in a typical polymer blend [1,24–27]. The nanoscale interphase properties of thermoset blends containing amphiphilic block copolymers are still far from being well understood [16], and further systematic investigations are still needed. Solid-state NMR (SSNMR) spectroscopy is a powerful method for characterizing the structure and dynamics of polymers [28–34]. A variety of novel solid-state NMR techniques have been successfully applied in elucidating the microdomain structure and dynamics in multiphase polymers in the past decade [35–41]. In spite of these previous studies, little NMR work has been reported on the systematic study of the evolution of phase behavior and microdomain structure in a series of polymer blends so far, especially the evolution of interphase under different conditions. In our previous work [16], we proposed a NMR method to quantitatively determine the interphase thickness in multiphase polymers, and the method was successfully applied to elucidate the influence of the volume fraction of PEO block on the nanoscale interphase and microdomain structure in 60/40 (w/w) ER/PEO–PPO–PEO blends. It was found that the interphase thickness is insensitive to the volume fraction of PEO block, whereas the domain size is sensitive, in these blends. However, the contribution of the rigid component to the interphase thickness was not considered in our previous model, therefore, the determined interphase thickness was slightly less than the actual value.

This study is a subsequent work of our previous SSNMR studies on the thermoset blends with amphiphilic PEO-containing triblock copolymers [16]. In this work, first, we improved the previously proposed NMR method to provide more accurate quantitative determination of interphase thickness and further verify the universality of this NMR method in different polymer blend systems. The improved method, in combination with other techniques, was then applied to elucidate the phase behavior, miscibility, heterogeneous dynamics and microdomain structure in UPR/PEO–PPO–PEO blends. The experimental results were compared with those of ER/PEO–PPO–PEO blends to systematically elucidate the influence of binary polymer–polymer interaction on the phase behavior, domain size and especially the interphase thickness in thermoset blends of UPR and ER, respectively, with the same PEO–PPO–PEO triblock copolymer at the same weight fraction. These NMR results were further compared with the previous theoretical prediction of interphase properties between two immiscible polymers proposed by Helfand et al. Based on the present study and our previous work, we proposed a model for the evolution of phase behavior and microstructure, especially the interphase properties, in thermoset blends of UPR and ER, respectively, with the same PEO–PPO–PEO triblock copolymer.

2. Experimental

2.1. Materials and preparation of samples

Poly(ethylene glycol)-*block*-poly(propylene glycol)-*block*-poly(ethylene glycol) triblock copolymers (PEO–PPO–PEO), EO30 and EO80 with average molecular weight (M_n) of 5800 and 8400, were purchased from Aldrich Chemical Co., Inc. The calibrated contents of ethylene glycol (EO) in EO30 and EO80 by ^{1}H liquid-state NMR of the two samples in $CDCl_3$ were 36 wt% and 79 wt%, respectively. The liquid uncured unsaturated polyester resin (UPR) was supplied by Tianjin HECAI Resin Co., Ltd. (China). It contains unsaturated polyester prepolymer and 35 wt% styrene as cross-linking monomer. The prepolymer ($M_w = 8700$ and polydispersity index of 2.9 as determined by gel permeation chromatography (GPC) (Waters)) is made from maleic anhydride, phthalic anhydride and propylene glycol at a molar ratio of 2:1:4 as determined by ^{1}H liquid-state NMR (Fig. 1). Benzoyl peroxide (BPO) (Aldrich Chemical Co., Inc.) was used as initiator. To allow a direct comparison of UPR/PEO–PPO–PEO with previous work on 60/40 (w/w) ER/PEO–PPO–PEO [16], two UPR/PEO–PPO–PEO blends with 40 wt% PEO–PPO–PEO block copolymers (EO30 and EO80) were used in this work. These two blends were denoted as UPR/EO30 and UPR/EO80, respectively, and prepared according to the following procedure. At 80 °C 40 wt% EO30 or EO80 was first dissolved in unsaturated polyester with continuous stir, then 0.5 wt % BPO initiator was added to the blend with continuous stirring until a homogeneous ternary mixture was obtained. The mixture was then immediately poured into an aluminum pan, degassed at 90 °C in vacuum, cured at 80 °C for 8 h, and then post-cured successively at 120 °C for 2 h and 150 °C for 2 h. The samples were allowed to cool to room temperature for study.

2.2. Differential scanning calorimetry (DSC) measurements

DSC Measurements were performed on a NETZSCH DSC 204 differential scanning calorimeter in a dry nitrogen atmosphere. Samples of about 8 mg were placed in the DSC pan. All samples were first heated to 100 °C from −60 °C at a rate of 20 °C/min (first heating scan) and kept at that temperature for 2 min; subsequently, they were cooled at a rate of −20 °C/min to detect crystallization

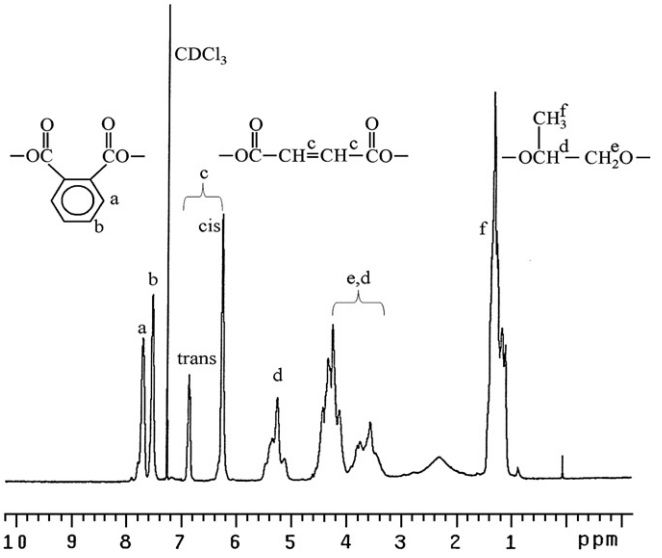

Fig. 1. The 400 MHz liquid-state ^{1}H NMR spectrum of the UPR prepolymer dissolved in $CDCl_3$. The assignment of the peaks and their corresponding chemical groups including maleic anhydride, phthalic anhydride and propylene glycol are denoted in the figure.

(cooling scan). Following the cooling scan, a second scan was conducted with the same heating rate as the first. The midpoint of the slope change of the heat capacity plot of the second heating scan was taken as the glass transition temperature (T_g). The crystallization temperature (T_c) was taken as the minimum of the exothermic peak, whereas the melting temperature (T_m) was taken as the maximum of the endothermic peak.

2.3. Transmission electron microscopy (TEM) experiment

TEM experiment was carried out on a FEI Tecnai-20 electron microscopy instrument. The specimens for TEM observation were prepared by microsectioning and were mounted on a copper grid, then stained in the vapor of an aqueous solution of RuO_4.

2.4 NMR experiments

NMR Experiments were performed on a Varian UNITYplus NMR spectrometer at a proton frequency of 400.2 MHz and at room temperature (25 °C). In the liquid-state NMR experiment, the sample was dissolved in $CDCl_3$. In the solid-state NMR experiments, the samples were placed in a zirconia rotor and a 5 mm CP/MAS probe was used. The magic angle spinning (MAS) frequencies were 8 kHz for dipolar filter experiments and 4.5 kHz for two-dimensional (2D) proton wide-line separation (WISE) NMR experiments. The ^{1}H and ^{13}C chemical shifts were referenced to external TMS and HMB (hexamethylbenzene), respectively. Solid-state NMR experiments used in this work are briefly described below, detailed experimental parameters and conditions for some of the pulse sequences can be found in our previous work [16].

(1) ^{1}H dipolar filter and spin diffusion NMR experiments were used to characterize the heterogeneous dynamics, phase behavior and quantitative microdomain structure of the blends [42,43]. Dipolar filter strength depends on the N_{cycle}, the times of the 12-pulse dipolar filter, and the interpulse spacing used in the experiments [16,44,45]. All spin diffusion experiments in this work were performed under static conditions to avoid any change of the spin diffusion coefficient under MAS.

(2) ^{1}H-to-^{13}C cross-polarization MAS NMR experiment (CP/MAS) was used to detect the signals of rigid component with high CP efficiency, and the recycle delay was 5 s. ^{13}C direct-polarization MAS NMR experiment (DP/MAS) with short recycle delay of 0.5 s was used to observe the signals of mobile component with short spin–lattice relaxation time (T_1) and suppress the rigid component with long T_1 [46]. The 90° pulse length was typically 4.5 μs and the CP contact time was 400 μs to minimize the spin diffusion among protons during CP.

(3) 2D ^{1}H-to-^{13}C WISE NMR experiment was used to characterize polymers with heterogeneous dynamics and complex morphology that includes hard and soft domains, especially, the degree of phase separation can be qualitatively determined [28,47]. Domains are distinguished by the ^{1}H wide-line spectrum (F1 dimension), broad if rigid and narrow if motionally averaged. Corresponding observed ^{13}C chemical shifts (F2 dimension) indicate the segmental composition of the regions. The experimental parameters are the same as those used in ^{13}C CP/MAS NMR experiment.

(4) ^{1}H dipolar filtered Hahn spin echo NMR experiments shown in Fig. 2 were employed to measure the transverse relaxation time (T_2) [48], which can be directly used to determine the proton spin diffusion coefficient for the mobile polymers as proposed by Mellinger et al. [49]. The experimental conditions of the dipolar filter sequence before Hahn spin echo are the same as that used in corresponding ^{1}H spin diffusion experiments.

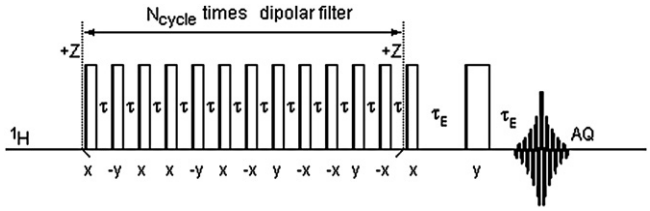

Fig. 2. Dipolar filtered Hahn spin echo pulse sequence to measure the T_2 of the mobile component.

3. NMR method

In our previous work on ER/PEO–PPO–PEO blends [16], we developed a NMR method based on ^{1}H spin diffusion experiments to quantitatively determine the interphase thickness in multiphase polymers containing rigid and mobile components. However, the contribution of the rigid component to the interphase thickness was not considered in that model, therefore, the determined interphase thickness was slightly less than its actual value. In this paper, we improved that method to provide a more accurate determination of the interphase thickness by considering the contributions of both the rigid and the mobile components. Detailed discussions of this NMR method can be found in Appendix.

4. Results and discussion

In our previous work [16], a variety of solid-state NMR methods were used to characterize nanostructured thermoset blends ER/EO30 and ER/EO80, and detailed information about the heterogeneous dynamics, miscibility and microdomain structures in these two blends were obtained. Because the chemical structure of UPR is significantly different from ER, the binary polymer–polymer interaction between thermoset resin and block copolymer should be changed and different phase behavior and microdomain structure could be observed in UPR/PEO–PPO–PEO and ER/PEO–PPO–PEO thermoset blends. In the following section, similar techniques used in Ref. [16] were employed here to elucidate the phase behavior, miscibility, heterogeneous dynamics and microdomain structure in UPR/PEO–PPO–PEO blends. We will closely compare the results of UPR/PEO–PPO–PEO blends to those of ER/PEO–PPO–PEO blends containing the same block copolymer.

4.1 PEO crystallinity, phase behavior, morphology and microdomain structure characterized by DSC, TEM experiments

Compatible polymer blends are usually diagnosed as such by their transparency and single T_gs from DSC experiment. These criteria are practical and imply a homogeneity on a scale of tens of nanometers or smaller [1]. However, it should be noted that there are a number of systems which exhibit phase separation but still have a single T_g. A single T_g does not always mean that the system is homogeneous and consists of a single phase. The obvious difference in transparency between 60/40 (w/w) cured UPR/EO30 and UPR/EO80 blends as shown in Fig. 3 suggests that the phase behaviors and miscibility in these two samples are quite different. The 60/40 UPR/EO30 is milk-white and opaque at even above the melting point of EO30 (39 °C) [16], which indicates that macrophase separation took place in this blend. On the contrary, the 60/40 UPR/EO80 is completely clear and transparent even at room temperature far below the melting point of EO80 (63 °C) [16]. On the basis of transparency, we can expect that the dispersed phase size in UPR/EO80 should be smaller than that in UPR/EO30. Compared with UPR/PEO–PPO–PEO blends, both ER/EO30 and ER/EO80 are transparent at room temperature, indicating the presence of microphase separation [9]. Since UPR/EO30 is macrophase

Fig. 3. Transparent property of the 60/40 (w/w) UPR/PEO–PPO–PEO blends: (left) UPR/EO30 and (right) UPR/EO80. The sample thickness is 2 mm and the two lightening words "NMR" are on the back of the two samples.

separation, we will focus our attention on elucidating the nanoscale microdomain structure of UPR/EO80 in the following sections.

Fig. 4 shows the DSC traces of the second heating scan and the cooling scan for EO80, cured UPR/EO80 at different EO80 contents and cured UPR. It is observed that the melt peak at $T_m = 63\ ^\circ C$ and crystalline peak at $T_c = 28\ ^\circ C$ of pure EO80 in Fig. 4a and b, respectively, gradually decrease and shift to low temperature with decreasing EO80 content, and disappear at about 40 wt% EO80 content. On the other hand, the glass transition temperature (T_g) of the blend, with a pure EO80 copolymer at $-56\ ^\circ C$, increases with decreasing EO80 content and is not well resolved, which could be only roughly estimated by taking the midpoint of the slope change of the heat capacity plot of the second heating scan. The above DSC results indicate that there exists polymer–polymer interaction between EO80 and UPR network in the 60/40 UPR/EO80. It should be also noted that although a small melting transition was still observed in Fig. 4a, the fraction of crystalline PEO in the blend was considerably small compared to that in pure EO80. Therefore, its influence on the following discussions is negligible. Although the blend could in reality be of microphase separation, it is hard to confirm the existence of the microphase separation only on the basis of the DSC results. In the following section, we will pay our main attention to 60/40 UPR/EO80, and a direct comparison between nanostructured UPR/EO80 and 60/40 ER/EO80 reported in our previous work [16] is made. Without special notation, the abbreviation of UPR/EO80 represents the 60/40 UPR/EO80 blend in the following discussion.

The morphology of UPR/EO80 was further investigated by TEM as shown in Fig. 5. The irregular nanoscale sphere-like morphology was clearly observed. The dark areas are PPO domains, because the PPO block was preferentially stained with RuO_4 compared to the cured UPR matrix. The size of the microdomain was of the order of 10–30 nm. Although TEM experiments can provide important information about the morphology and microdomain structure of UPR/EO80, it is difficult for TEM to directly determine the interphase thickness or chemical composition in the interphase region of such samples with irregular spherical-like morphology. These informations will be further elucidated in the following NMR experiments.

4.2. Heterogeneous dynamics, miscibility and phase behavior determined by ^1H MAS, dipolar filter and ^{13}C MAS NMR experiments

^1H NMR spectrum reflecting dipolar coupling among protons is a convenient method to monitor the heterogeneous dynamics and phase behavior of polymer blends [28,50,51]. Fig. 6 shows the static ^1H spectra of UPR/EO80. Since the glass transition temperatures for amorphous PEO and PPO are well below the ambient temperature, the narrow peaks ($\sim$2 kHz fwhm) at the center and the relative broad hump ($\sim$39 kHz fwhm) at the bottom of the spectra can be assigned to the mobile (PEO and PPO) blocks in EO80 and rigid cross-linked UPR network, respectively. The remarkable dynamic difference between the UPR and the EO80 copolymers shown in

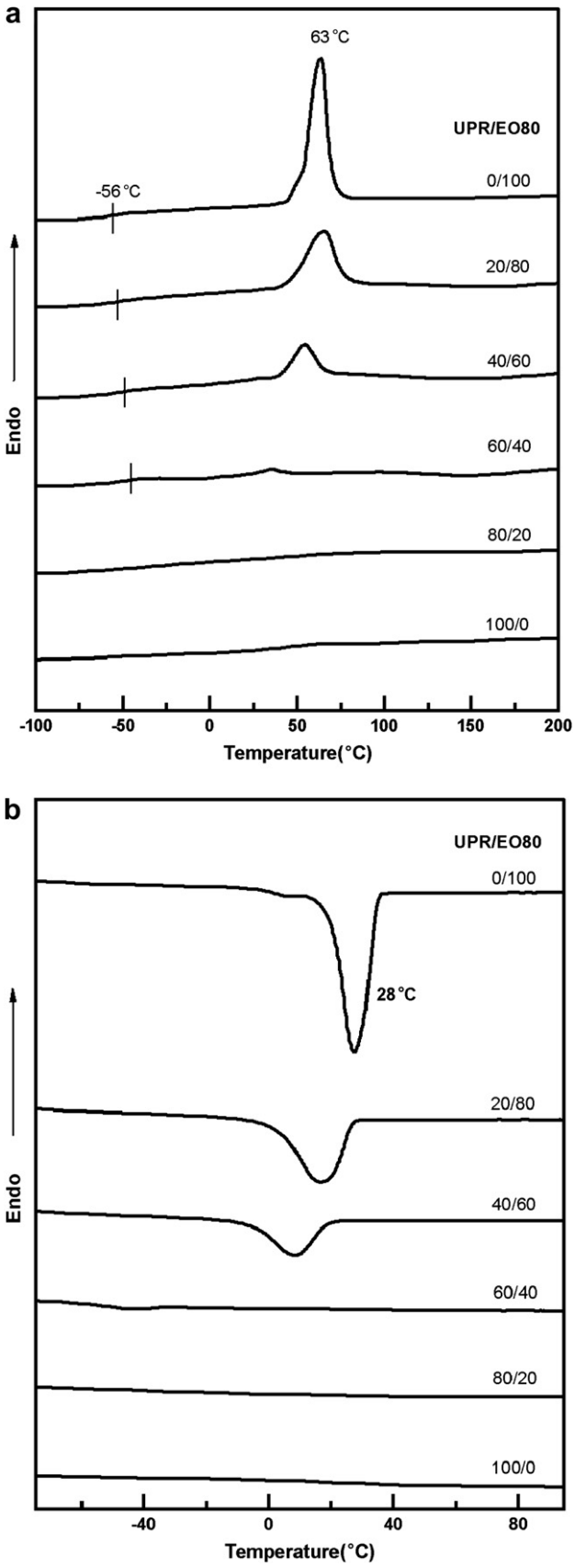

Fig. 4. DSC traces of EO80, cured UPR/EO80 at different EO80 contents and cured UPR: (a) the second heating scan and (b) the cooling scan.

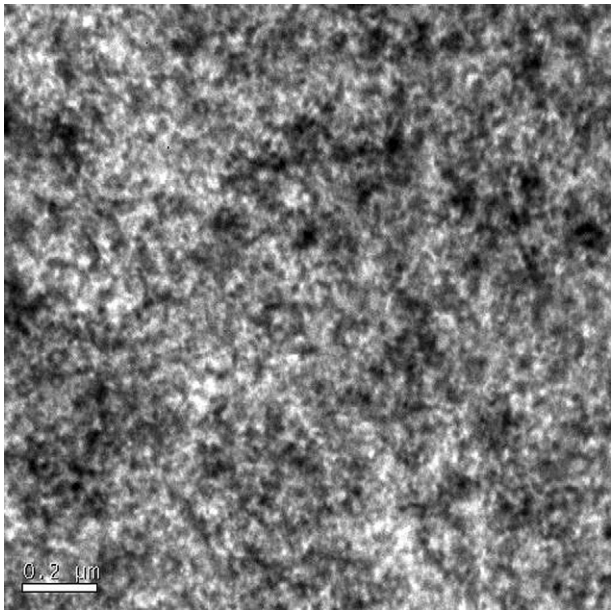

Fig. 5. TEM micrograph of UPR/EO80. The specimen for TEM observation was stained with RuO_4 and the scale bar is 200 nm.

Fig. 6 indicates the presence of phase separation in this blend. Fig. 7 shows the expanded ^{1}H MAS NMR spectra of EO80 and UPR/EO80 acquired with 8 kHz MAS. The narrow peak at around 3.5 ppm was assigned to the overlapped peaks of the methylene protons of PEO and the methine and methylene protons of PPO blocks, and the peak at 1.1 ppm was assigned to methyl protons of PPO block. It is noteworthy that the intensity ratio of the peak at 3.5 and 1.1 ppm for UPR/EO80 is much larger than that of EO80, indicating a much larger amount of PEO is mobile in UPR/EO80 than in EO80. This result is consistent with that from DSC experiments shown in Fig. 4 and confirms again that the formation of crystalline domains of PEO block in UPR/EO80 is inhibited. On the contrary, a large fraction of PEO block in pure EO80 is crystalline.

^{1}H dipolar filter experiment is another powerful method to provide more detailed information about the heterogeneous dynamics, miscibility and microdomain structure in polymer blends composed of rigid and mobile phases [42,49,50]. By increasing the dipolar filter strength, the broad peaks arising from protons in immobilized and rigid region can be suppressed. Fig. 8 shows the ^{1}H dipolar filtered NMR spectra of UPR/EO80 under 8 kHz MAS. A

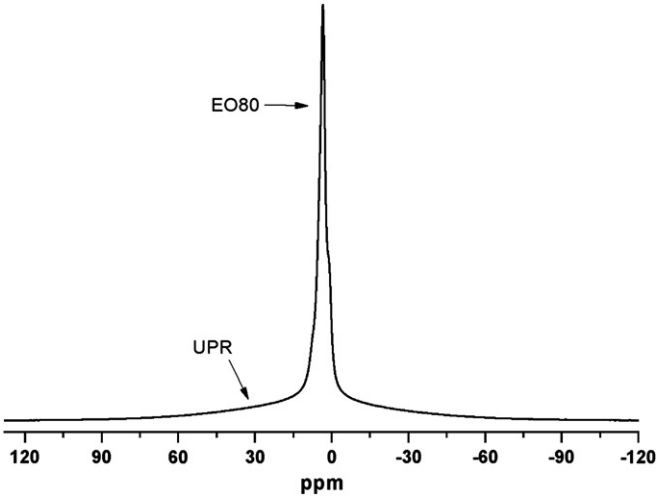

Fig. 6. ^{1}H static NMR spectrum of UPR/EO80.

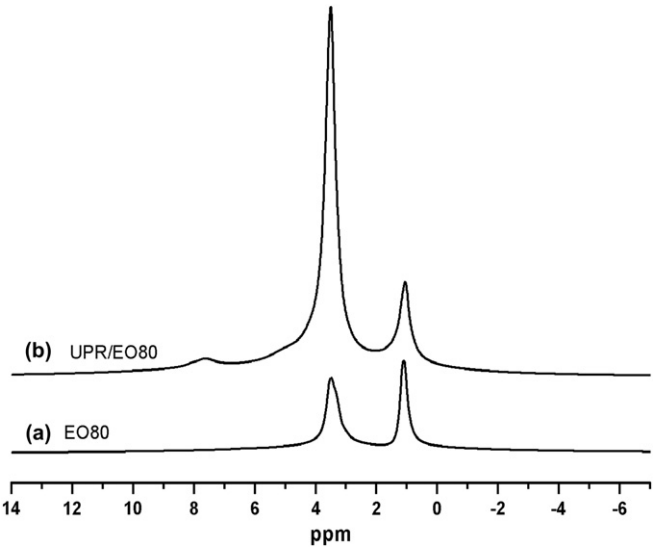

Fig. 7. The expanded ^{1}H MAS NMR spectrum of (a) EO80, and (b) UPR/EO80 at 8 kHz MAS. The side bands were out of this region.

superposition of broad and narrow lines is observed in MAS spectrum without dipolar filter ($N_{cycle} = 0$). The line width of the broad component was far less than that of the rigid UPR phase (~39 kHz fwhm), thus the broad line can be reasonably assigned to the protons of the "immobilized" interphase [16]. With increasing N_{cycle}, the proton signal in the interphase region was obviously suppressed and only the proton signal of the mobile phase with weak dipolar coupling remained. In addition, we can also observe a weak and broad peak at about 7–8 ppm in Fig. 8 without dipolar filter, this peak can be remarkably suppressed with increasing dipolar filter strength. We suggest that this peak should be attributed to the partially cured UPR intimately mixing with the immobilized amorphous PEO in the interphase region, and this result is very similar to that found in ER/EO80 blend [16]. It should be mentioned here that propylene glycol in UPR was total rigid (^{1}H static NMR spectrum of cured UPR is not shown here), therefore, the signal for these short propylene glycol groups does not contribute to the signal that we assign to the mobile phase.

Compared with ^{1}H NMR, ^{13}C NMR technique is another effective way to study the dynamics and microstructure of polymers due to its excellent resolution; thus it was applied to characterize the

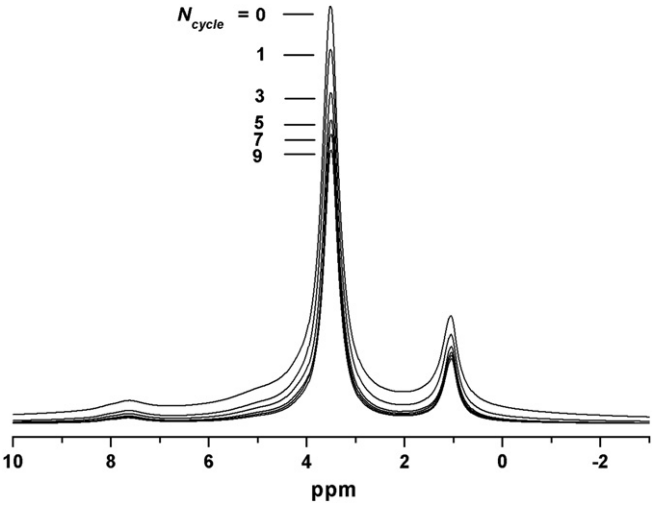

Fig. 8. ^{1}H dipolar filtered MAS spectra of UPR/EO80 at 8 kHz MAS. The filter strength is increased by increasing N_{cycle} in dipolar filter pulse sequence [16].

molecular mobility and phase behavior of UPR/EO80 blend. In general, ^{1}H-to-^{13}C CP/MAS experiment can predominantly detect the signals from the rigid component due to its high CP efficiency. Whereas ^{13}C DP/MAS experiment with a short recycle delay time can detect signals from only the mobile component and suppress the rigid one. Therefore, the rigid segments exhibit strong signals in the ^{13}C CP/MAS spectrum, while the mobile segments show narrow and strong signals in the ^{13}C DP/MAS spectrum. Fig. 9 shows the ^{13}C DP/MAS spectra of EO80 and UPR/EO80, and the ^{13}C CP/MAS spectrum of UPR/EO80 at 4.5 kHz MAS. In the ^{1}H MAS NMR spectrum shown in Fig. 7, the peaks of the mobile PEO and PPO at 3.5 ppm are seriously overlapped and cannot be distinguished. However, the methylene carbon of PEO at 70–72 ppm and methine, methylene and methyl carbons of PPO at 72, 74, and 16 ppm, respectively, can be well distinguished in ^{13}C DP/MAS NMR spectra shown in Fig. 9. On comparing the ^{13}C DP/MAS spectra in Fig. 9a and b, it is noteworthy that the relative intensity of the sharp peak of amorphous PEO at 70 ppm in UPR/EO80 is remarkably stronger than that in EO80, indicating that most of PEO in UPR is segregated from the cured UPR network upon curing and forming the mobile phase, whereas most of PEO in EO80 is in crystalline region. This result is consistent with those obtained from DSC and ^{1}H MAS NMR experiments. Three narrow PPO peaks are also clearly seen, which indicates that PPO block is also repelled from the rigid UPR network. The strong signals with narrow line widths in the DP/MAS spectrum of UPR/EO80 (Fig. 9b) indicate that these segments undergo fast motions in the mobile phase. In addition, a small mobile phenyl anhydride signal at 128 ppm in UPR is also observed in Fig. 9b, which should be attributed to the partially cured UPR signals in the interphase region that was intimately mixed with PEO. This signal also confirms the existence of the interphase in this blend. In Fig. 9c, different groups of the rigid cured UPR phase can be observed in the ^{13}C CP/MAS spectrum due to the strong ^{1}H–^{13}C dipolar coupling.

4.3. Correlation of mobility and microphase structure determined by 2D ^{1}H–^{13}C WISE experiments

2D WISE NMR experiment has been widely used for determining heterogeneous dynamics in solid polymers [28,47]. It can be used to determine the degree of phase separation and allows one to qualitatively characterize whether there is an extended interphase between the two phases in phase-separated blends. In addition, the obtained line widths of individual components from 2D WISE spectroscopy can also be used to calculate the spin diffusion coefficient needed for the determination of the domain size. Fig. 10 shows the ^{1}H slice projection of 2D ^{1}H–^{13}C WISE NMR spectrum for different groups of UPR/EO80 blend. It was found that the PEO peak at 70 ppm exhibits a strong and narrow peak at the center and a small broad peak at the bottom of the spectrum. The narrow peak should be assigned to the mobile PEO blocks segregated from the cured UPR matrix, indicating that PEO block is only weakly miscible with cured UPR network. Since PEO was almost amorphous in this blend from DSC results, the small broad peak should be reasonably attributed to the immobilized PEO in the interphase region. In contrast with UPR/EO80, the slice projection of PEO from WISE experiments for ER/EO80 and ER/EO30 clearly indicates the presence of a thick interphase in these blends, and a large percentage of PEO was intimately mixed with ER in the interphase region [16]. In Fig. 10, the slice projection of PPO peak at 74 ppm in UPR/EO80 only shows a narrow peak, indicating that the PPO block was immiscible with UPR and completely segregated from the cured UPR network upon curing. In addition, from the slice projection of UPR at 128 ppm, we can observe a superposition of a broad line and a small narrow line. The narrow line should be attributed to the immobilized UPR component in the interphase region, while the broad line should be attributed to the cured UPR network. The above WISE NMR results provide a direct evidence of the existence of a small interphase containing PEO in UPR/EO80, which is in good agreement with those obtained by 1D ^{1}H and ^{13}C NMR experiments. A quantitative determination of the interphase thickness will be performed from the ^{1}H spin diffusion experiments in the following section.

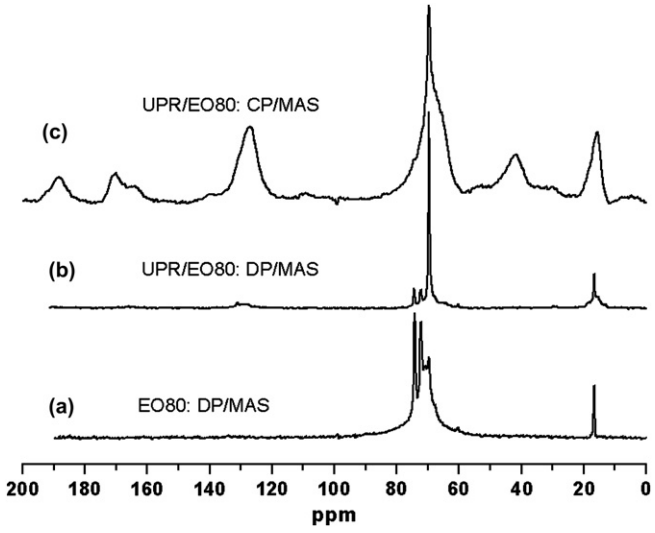

Fig. 9. ^{13}C DP/MAS spectra of (a) EO80, (b) UPR/EO80, and (c)^{13}C CP/MAS spectrum of UPR/EO80.

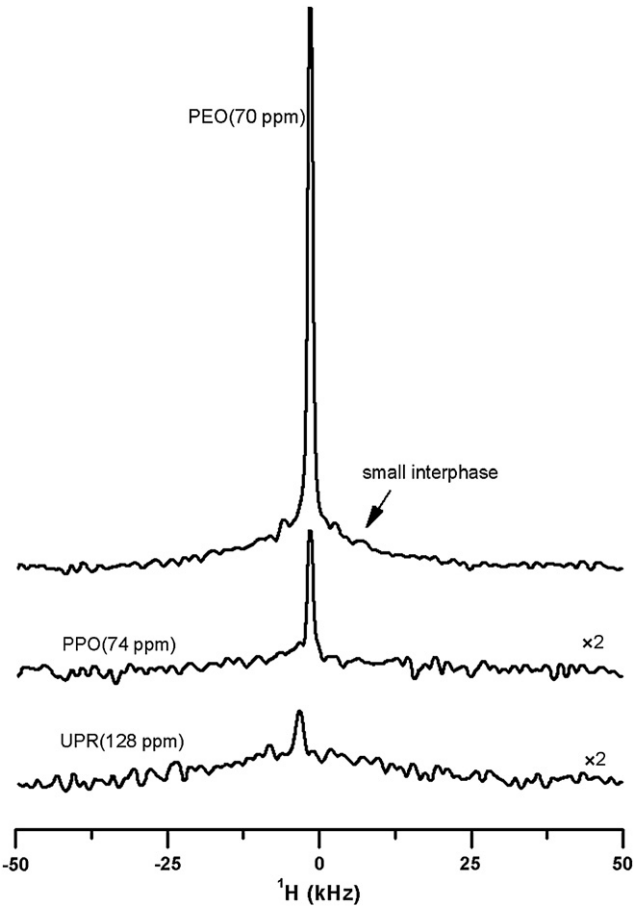

Fig. 10. ^{1}H slice projections of 2D ^{1}H–^{13}C WISE NMR spectrum for different groups of UPR/EO80 blend.

Table 1
Proton fractions of EO80 in UPR/EO80, as well as the proton fractions of PPO in EO80 and UPR/EO80 determined by ^{1}H liquid-state NMR in $CDCl_3$

Samples	UPR/EO80	EO80
Proton fraction of PEO–PPO–PEO copolymer (stoichiometric proton ratio) (%)	54.4	–
Proton fraction of PPO in UPR/EO80 and EO80 (%)	10.9	21.4

4.4. Determination of the interphase thickness and domain size by ^{1}H spin diffusion experiments

To get a better understanding of the phase separation in UPR/EO80, we need to know detailed and quantitative structural information concerning the domain size and interphase thickness. On the basis of the improved NMR method to measure the interphase thickness (Eq. (11) in the Appendix), we can directly determine the interphase thickness in UPR/EO80 by ^{1}H spin diffusion NMR experiments. Table 1 lists all the measured stoichiometric proton ratio of the block copolymer EO80 in UPR/EO80 using ^{1}H liquid-state NMR, together with the proton fraction of PPO in EO80, which will be used to determine the fraction of PEO in the mobile phase and the interphase region.

Fig. 11a shows the ^{1}H spin diffusion curves with increasing N_{cycle} for UPR/EO80. On the basis of the strategy proposed by Spiess et al. [28,49], the signal intensities were corrected to eliminate the effect of spin–lattice relaxation (T_1) on the measurement of spin diffusion

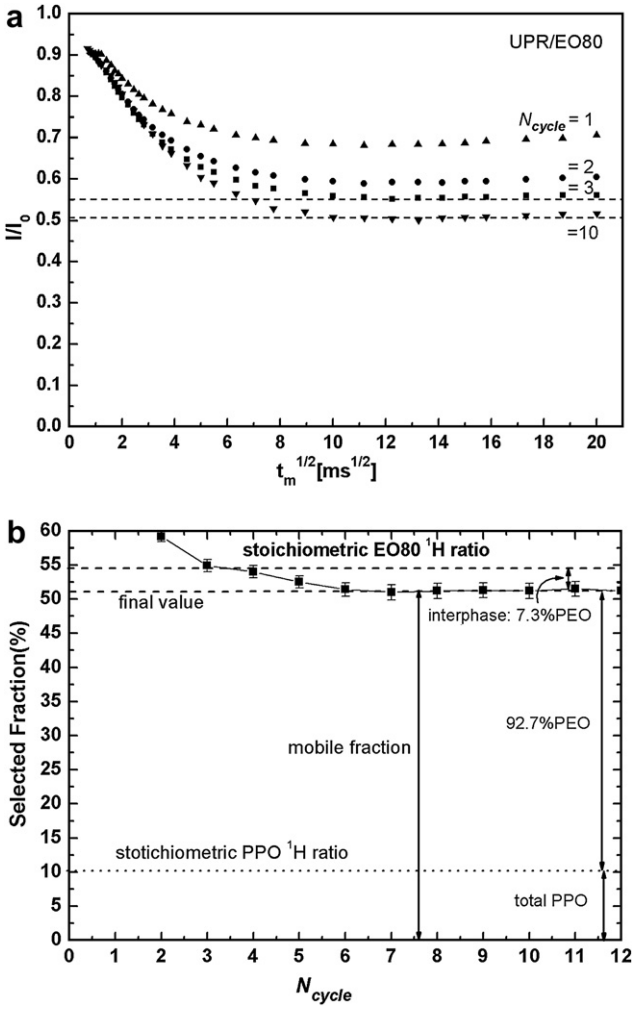

Fig. 11. ^{1}H spin diffusion experiments for UPR/EO80: (a) static spin diffusion curves of UPR/EO80 at different filter strengths (N_{cycle}); (b) selected ^{1}H fraction of UPR/EO80 as the function of filter strength (N_{cycle}).

using the multiplicative factor $\exp(+t_m/T_1)$. It should be emphasized that the quantitative results depend on the accurate measure of the signal intensity at zero mixing time ($t_m = 0$) which can reliably be linearly extrapolated from the initial data points within small mixing times as reported in previous work [49]. The two dashed lines denote the different end values, i.e., the selected fraction, of the spin diffusion curves at $N_{cycle} = 3$ and 10, respectively. When $N_{cycle} = 3$, the corresponding equilibrium value (54.4%) is just the stoichiometric proton ratio of EO80 in UPR/EO80. When $N_{cycle} > 6$, the equilibrium value at different N_{cycle} is kept unchanged, which is the final value (f_m) we need. Fig. 11b shows the N_{cycle} dependence of the selected fraction in spin diffusion experiments for UPR/EO80. The final value f_m (=51.2% at $N_{cycle} > 7$) is slightly lower than that expected from the stoichiometric proton ratio (54.4%). Comparing Fig. 11b with Fig. 15, we obtain that about 7.3% (f_i) immobilized PEO is in the interphase region, while the rest 92.7% mobile PEO and all PPOs are expelled from the cured UPR network. The above quantitative NMR results confirm the existence of a small interphase region in this blend. Since $f_m = 51.2\%$ and $f_{sm} = 54.4\%$, we can obtain $\lambda_{DFS} = f_m/f_{sm} = 51.2/54.4 = 0.94$, which is very close to the value (1.0) of ideal phase separation without interphase, therefore, we can conclude that this blend exhibits strong phase separation.

If we neglect the slight difference of the proton density of PEO and PPO in EO80, the interphase thickness in UPR/EO80 can be directly estimated from Eq. (11). The dimensionality in Eq. (11) was chosen as $p = 3$ (sphere-like) on the basis of the foregoing TEM micrograph, thus we obtain $d_{itp} = 0.02 d_{dis}$ from Eq. (11). Since the estimated domain size of the dispersed phase (d_{dis}) from TEM micrograph shown in Fig. 5 was in the range of 10–30 nm, we have $d_{itp} = 0.2$–0.6 nm. It is noteworthy that the interphase thickness (d_{itp}) measured here combining simple ^{1}H spin diffusion experiment with TEM technique does not require spin diffusion simulation and the knowledge of the spin diffusion coefficients of the sample which are needed in traditional NMR methods [28,49,51].

Alternatively, we can also use traditional NMR strategy to determine d_{dis} if SAXS and TEM cannot provide quantitative structural information due to either lower electron density contrast or low stain contrast between different phases, such as the case for ER/EO80 in our previous work [16]. By measuring the rate of proton spin diffusion following the dipolar filter in spin diffusion experiment, the domain size of the dispersed phase A in the two-phase A/B blend, d_{dis}, can be determined by the following equation [28,52,53]

$$d_{dis} = \frac{4\varepsilon\sqrt{D_A D_B}}{\sqrt{\pi}\left((\rho_A^H/\rho_B^H)\sqrt{D_A} + \sqrt{D_B}\right)}\sqrt{t_m^{s,0}} \quad (1)$$

where ε (=1–3) has the same meaning as p used in Eq. (11), and its value depends on the morphology; $t_m^{s,0}$ is the characteristic mixing time of spin diffusion introduced by Mellinger et al. [49], and it can be determined by the intercept of the extrapolated linear initial decay with the x-axis in spin diffusion curve as shown in Fig. 12; and ρ_A^H and ρ_B^H are proton densities of the two phases, respectively. The diffusion coefficient of the mobile phase (D_A) can be calculated from the following equations proposed by Mellinger et al. [49] through transverse relaxation time (T_2) measurements:

$$D_A\left(T_2^{-1}\right) = \left(8.2\times10^{-6}T_2^{-1.5} + 0.007\right)\ \mathrm{nm^2/ms},\quad 0 < T_2^{-1} < 1000\ \mathrm{Hz} \quad (2)$$

$$D_A\left(T_2^{-1}\right) = \left(4.4\times10^{-5}T_2^{-1} + 0.26\right)\ \mathrm{nm^2/ms},\quad 1000 < T_2^{-1} < 3500\ \mathrm{Hz} \quad (3)$$

The diffusion coefficient of the rigid phase can be calculated from the following equation that is valid for the Gaussian line shape [54]:

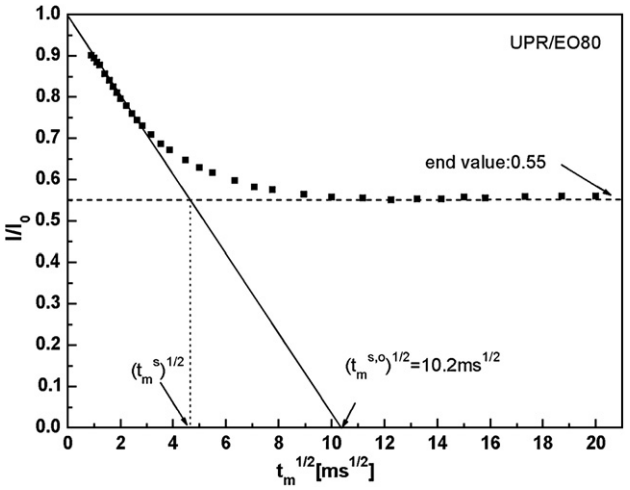

Fig. 12. Spin diffusion curve of UPR/EO80 at $N_{cycle} = 3$, plotted as the normalized intensity I/I_0 against the square root of the mixing time t_m. The extrapolated value $t_m^{s,0}$ is estimated and denoted in the figure. The value t_m^s used in Ref. [49] is also denoted.

$$D_B = \frac{1}{12}\sqrt{\frac{\pi}{2\ln 2}}\langle r^2\rangle \Delta\nu_{1/2}^B \quad (4)$$

where $\langle r^2\rangle$ is the mean-square distance between the nearest spins (typically of the order of 0.04–0.06 nm^2 in polymer), $\Delta\nu_{1/2}^B$ is the line width of proton wide-line signals obtained by either 2D WISE experiment of rigid phase or deconvolution of the wide-line ^{1}H NMR spectrum [55].

To obtain the domain size of the dispersed phase for UPR/EO80, we select the spin diffusion curve at $N_{cycle} = 3$ as shown in Fig. 12, which gives the corresponding equilibrium (end) value at the stoichiometric proton ratio (54.4%) of EO80 in UPR/EO80. The initial linear portion of the curve is linearly extrapolated to give a value of 10.2 ms$^{1/2}$ for $(t_m^{s,0})^{1/2}$. Table 2 lists all the parameters required for the spin diffusion calculations. The calculated spin diffusion coefficients for the mobile and rigid phases are 0.11 and 0.31 nm^2/ms, respectively, which are in good agreement with that reported in previous literature [56,57]. It should be noted that the calculated spin diffusion coefficient of the rigid phase (0.31 nm^2/ms) is obviously lower than that reported in some literature for rigid systems (0.8 nm^2/ms); this disagreement is due to the difference in the full line width at half height (compare $\Delta\nu_{1/2}^B$ = 76 kHz from Ref. [47] with the corresponding $\Delta\nu_{1/2}^B$ estimated for UPR/EO80). A similar spin diffusion coefficient of the rigid phase for nylon-6 fibres was also reported [58]. Using the values given in Table 2, the domain size, interphase thickness and the long period for UPR/EO80 are calculated and listed in Table 3. The calculated domain size and the long period are about 14 and 16 nm, respectively, which are in agreement with the corresponding TEM result. It should be noted that the TEM only shows a wide dispersion of the domain size in the range of 10–30 nm and the extremely small interphase cannot be clearly seen. However, the NMR method has the advantage of yielding an average domain size of 14 nm for the sample, and the interphase thickness can then be directly determined by $d_{itp} = 0.02d_{dis} = 0.3$ nm. It should be emphasized here that the TEM technique is difficult to directly detect such small interphase in UPR/EO80, especially to provide the quantitative information on the PEO block in the interphase region.

Table 2
Volume fraction, line width, spin–spin and spin–lattice relaxation times, spin diffusion coefficients, and equilibrium mixing time used to calculate the domain size and interphase thickness

Parameters[a]	ϕ_m	T_2 (ms)	$\Delta\nu_{1/2}^B$ (kHz)	D_A (nm^2/ms)	D_B (nm^2/ms)	T_1 (s)	$(t_m^{s,0})^{1/2}$ (ms$^{1/2}$)
UPR/EO80	0.44	1.9	39	0.11	0.31	0.63	10.2

[a] ϕ_m is the volume fraction of EO80 in the blend, which can be calculated from the 60:40 weight ratio of UPR and EO80, as well as the density of UPR and EO80 of 1.23 and 1.05 g/cm^3, respectively. T_2 was measured by dipolar filtered Hahn spin echo pulse sequence as shown in Fig. 2. T_1 was measured by means of the inversion recovery method.

Table 3
Domain size (d_{dis}), long periods (d_{long}) and interphase thickness (d_{itp}) for UPR/EO80, ER/EO80 and ER/EO30 measured by ^{1}H spin diffusion experiments

Samples[a]	ε	d_{dis} (nm)	d_{long} (nm)	d_{itp} (nm)
UPR/EO80	3	14.2	16.2	0.3
ER/EO80	2	2.7	4.3	0.7
ER/EO30	2	8.9	14.4	1.1

[a] For ER/EO80 and ER/EO30, d_{dis} and d_{long} were determined in our previous work [16], while d_{itp} was recalculated in this article using the improved Eq. (11).

For the convenience of comparison between thermoset blends of ER and UPR, respectively, with the same PEO–PPO–PEO block copolymer in the following discussion, we also recalculated the interphase thickness in ER/PEO–PPO–PEO thermoset blends reported in our previous work [16] to give more accurate results. On the basis of the definition of λ_{DFS} and our previous experimental results, we obtained $\lambda_{DFS} = 22.2/39.9 = 0.56$ and $30.9/41.4 = 0.75$ for ER/EO80 and ER/EO30, respectively. Since the domain sizes of these two blends determined by NMR experiments were 2.7 and 8.9 nm, respectively [16], the corresponding corrected interphase thicknesses ($p = 2$ in Eq. (11)) for these two blends were 0.7 and 1.1 nm, respectively. It is noteworthy that the interphase thicknesses in ER/EO30 and ER/EO80 are considerably larger than that in UPR/EO80, indicating the phase separation in these two different thermoset blend systems are quite different.

4.5. Comparison of the phase behavior and microdomain structure between thermoset blends of UPR and ER, respectively, with the same PEO–PPO–PEO triblock copolymer

One aim of this work is to gain better understanding on the influence of different binary component interactions on the phase behavior and microdomain structure in blends of UPR and ER, respectively, with the same block copolymer. Therefore, it is important to compare the experimental results between these two different thermoset blend systems. The Flory–Huggins interaction parameter, χ, is widely used in the literature to describe the binary interactions of polymer blends [59], and is known to be the key factor controlling the final structure and properties of the phase-separated blends [1,21,60]. On the basis of the self-consistent mean-field theory, Helfand and co-workers predicted a quantitative relationship between interphase thickness (d_{itp}) and the thermodynamic interaction parameter χ [21]:

$$d_{itp} = \frac{2b}{(6\chi)^{0.5}} \quad (5)$$

where b is the Kuhn segmental length ($\sim$0.8 nm) [1]. Although the value of interaction parameter χ between the cross-linked thermoset resin and PEO–PPO–PEO block copolymers cannot be directly determined by means of the traditional methods [59,61,62], our NMR experimental results can provide qualitative supporting of the above relationship in thermoset blends with block copolymers.

First, it is expected that with increasing the thermodynamic interaction between the block copolymer and the cured-thermoset resin in the blends (increasing χ), the interphase thickness

should decrease. Due to different chemical structures of the UPR and ER, we can expect that the value of χ in these two different blend systems should be different. It is well known that there are strong hydrogen bonding interaction between the hydroxyl (–OH) of ER and the ether group (–O–) of PEO [59,61]. However, besides the end hydroxyl groups of UPR, there are less specific interaction groups between UPR and PEO than that between ER and the PEO block. Therefore, we can reasonably infer that the interaction parameter χ in UPR/PEO–PPO–PEO should be larger than that in ER/PEO–PPO–PEO. On the basis of Helfand's theory, it is expected that the interphase thickness in ER/PEO–PPO–PEO should be larger than that in UPR/PEO–PPO–PEO. Compared with ER/PEO–PPO–PEO blends, different phase behavior, miscibility, morphologies, domain size and interphase thickness were observed in UPR/PEO–PPO–PEO blends containing the same block copolymer. It was found that macroscopic phase separation took place in UPR/EO30, which was obviously different with the phase behavior of ER/EO30, where microphase separation took place. Due to the much higher PEO content in EO80, UPR/EO80 blend is not macroscopically phase-separated and exhibits nanostructure spherical-like morphology with large domain size of 14 nm. All NMR experiments including ^{1}H dipolar filter, WISE and spin diffusion experiments indicate that only a small fraction of PEO was mixed with UPR which forms the interphase region, and the calculated interface thickness is considerably small ($\sim$0.3 nm). Nearly most of the PEO block (93%) was repelled from the UPR matrix, which indicates that PEO is only weakly miscible with the cross-linked UPR network, and the UPR/PEO–PPO–PEO blends exhibit strong phase separation. On the contrary, due to the strong hydrogen bonding interaction between PEO block and cured ER network [63], PEO block is well miscible with ER network, therefore, both ER/EO30 and ER/EO80 exhibit weak phase separation. The interphase contains large amount of PEO block and the determined interphase thicknesses of ER/EO80 and ER/EO30 are 0.7 and 1.1 nm, respectively, which is considerably larger than that in UPR/EO80 (0.3 nm), while their domain sizes are obviously small of about 3 and 9 nm, respectively. It is also noted that the phase-separated morphology was changed from cylinder in ER/PEO–PPO–PEO [16] to sphere-like in UPR/PEO–PPO–PEO due to the increase of the binary component interaction.

Second, from Helfand's theory (Eq. (5)), it is also expected that the interphase thicknesses should kept unchanged if the thermodynamic interaction between the block copolymer and cured-thermoset resin remains unchanged. It was found in our previous work [16] that although the domain size increases from 3 nm in ER/EO80 to 9 nm in ER/EO30 with decreasing the PEO content in the PEO–PPO–PEO block copolymers, the interphase thicknesses (0.7 and 1.1 nm) are only slightly changed in these blends; this can be understood considering that the interaction parameter χ between the PEO block and cross-linked ER almost keeps unchanged. Our NMR results also demonstrate that the domain sizes depend strongly on the PEO fraction of the block copolymer in both ER/PEO–PPO–PEO and UPR/PEO–PPO–PEO blends. From the above discussion, we can reasonably suggest that the different thermodynamic interactions between the block copolymer and cross-linked thermoset resin and the PEO fraction of the block copolymer are the two key factors that control the phase behavior, miscibility, domain size and interphase thickness of these blends. Our systematic NMR results on UPR and ER thermoset blends are qualitatively in good agreement with the theoretical prediction of Helfand and Tagami [21].

It was mentioned in the foregoing discussion that the parameter λ_{DFS} as determined by ^{1}H spin diffusion NMR experiments can be used to characterize the extent of the phase separation in multiphase polymers. $\lambda_{DFS} = 1$ means strong phase separation in the blend, whereas $\lambda_{DFS} = 0$ means complete miscibility of the two components; if λ_{DFS} is obviously less than 1, this indicates that weak phase separation takes place in the blend. Since the obtained λ_{DFS} for ER/EO80 and UPR/EO80 were 0.56 and 0.94, respectively, these two samples are obviously the two typical model systems with weak and strong phase separations as shown in Fig. 13. These model systems enable us not only to obtain an overall understanding of the phase behavior, miscibility and structure evolution under different polymer–polymer interactions in thermoset blends with block copolymers, but also to verify the universality of the improved NMR methods proposed in our work in determining the interphase thickness in multiphase polymers. Our systematic NMR work on thermoset blends of UPR and ER, respectively, with PEO–PPO–PEO block copolymers clearly demonstrates that our method is robust even for multiphase polymer systems having strong phase separation with extremely small interphase region. On the basis of the above discussion, a possible model for the influence of binary component interaction (χ) and volume fraction of PEO (ϕ_{PEO}) on the phase behavior, miscibility, morphology, domain size and interphase thickness in thermoset blends of UPR and ER, respectively, with PEO–PPO–PEO triblock copolymer could be suggested as shown in Fig. 14, and a clear physical picture about evolution of phase behavior and microdomain structure in these thermoset blends with PEO-containing block copolymers can be achieved.

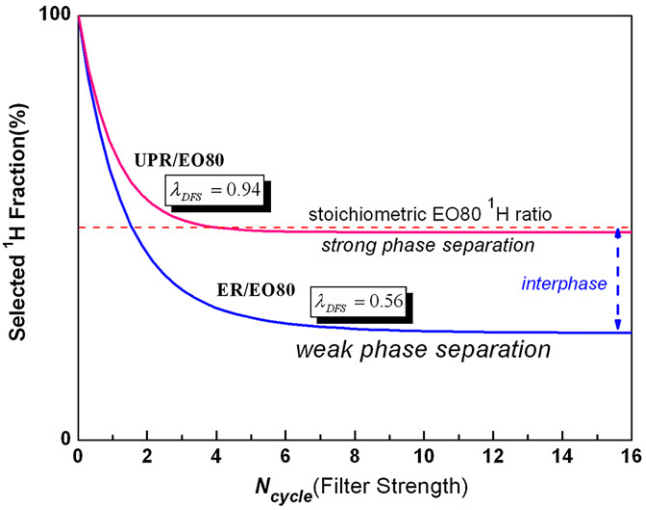

Fig. 13. Schematic illustration for typical strong and weak phase separations with small and large interphases in UPR/EO80 and ER/EO80 [16] thermoset blends, respectively, as determined by solid-state NMR experiments.

5. Conclusions

In this work, first, we improved the NMR method proposed in our previous work to provide more accurate determination of interphase thickness in multiphase polymers. In combination with other techniques, this improved NMR method was then applied to elucidate the phase behavior, miscibility, heterogeneous dynamics and microdomain structure in UPR/PEO–PPO–PEO thermoset blends. The experimental results were compared with those of ER/PEO–PPO–PEO blends to systematically elucidate the influence of different binary polymer–polymer interactions on the phase behavior, domain size and especially the interphase thickness in thermoset blends of UPR and ER, respectively, with the same PEO–PPO–PEO triblock copolymer. For UPR/EO80 blend, 1D and 2D NMR experiments show a distinct dynamic difference between UPR and EO80, indicating that the presence of phase separation and the formation of crystalline domains in PEO block were inhibited.

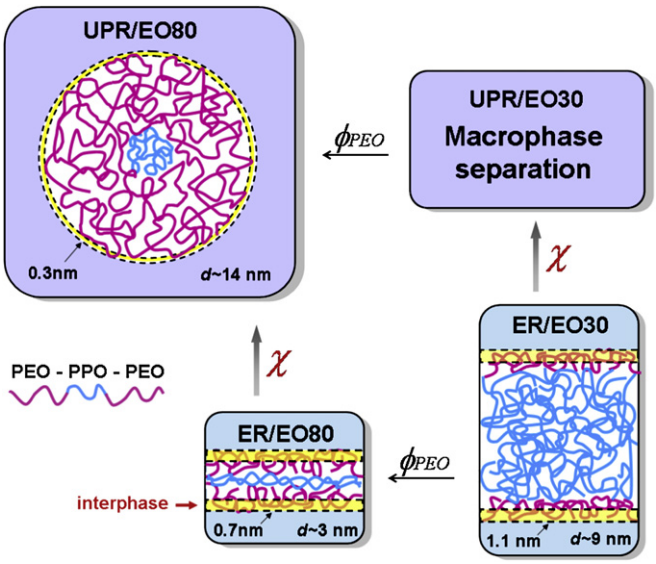

Fig. 14. Schematic illustration of the suggested model for the influence of binary component interaction (χ) and volume fraction of PEO block (ϕ_{PEO}) on the phase behavior and microdomain structure in blends of UPR and ER with PEO–PPO–PEO triblock copolymer. Yellow region with dotted line border represents the interphase region, and the interphase thickness and domain size (d) are also denoted in this figure (for interpretation of the references to colour in this figure legend, the reader is referred to the web version of this article).

Quantitative ^{1}H spin diffusion experiments reveals that only 7.3% PEO were immobilized and mixed with partially cured UPR that formed the interphase region, and the calculated interphase thickness and domain size were about 0.3 and 14 nm, respectively. These results indicate that PEO blocks were only weakly miscible with cured UPR matrix and the blend exhibits strong microphase separation. Upon curing, the cross-linked rigid UPR formed a separated microphase, while a large amount of mobile PEO was locally expelled from the cured UPR matrix and formed another microphase with mobile PPO. On the contrary, macrophase separation took place in UPR/EO30 due to the lower PEO content in EO30 compared to EO80. The observed phase behavior, morphologies and microdomain structure in blends of UPR and ER, respectively, with the same triblock copolymer are obviously different. The later has a larger interphase region containing considerable amount of PEO intimately mixing with cured ER network, indicating the presence of weak microphase separation and good miscibility between PEO block and cured ER network. It is suggested that the thermodynamic interaction between the block copolymer and cross-linked thermoset resin is the key factor that controls the phase behavior, morphology, domain size and interphase thickness of these thermoset blends. The NMR results are qualitatively in good agreement with the theoretical prediction of the interphase properties between two immiscible polymers proposed by Helfand et al. To our knowledge, this is the first systematic NMR study on the evolution of the phase behavior and detailed microstructure on the basis of determined interphase thickness by controlling the binary thermodynamic interactions. Our NMR works on different thermoset blend systems with weak and strong microphase separations clearly demonstrate that the improved NMR method is a general and useful tool to elucidate the phase behavior and subtle microdomain structure in multiphase polymers, and these information are of great importance for guideline of tailoring the nanostructure and morphologies in thermoset blends and therefore developing advanced polymer blends with desired physical and chemical properties.

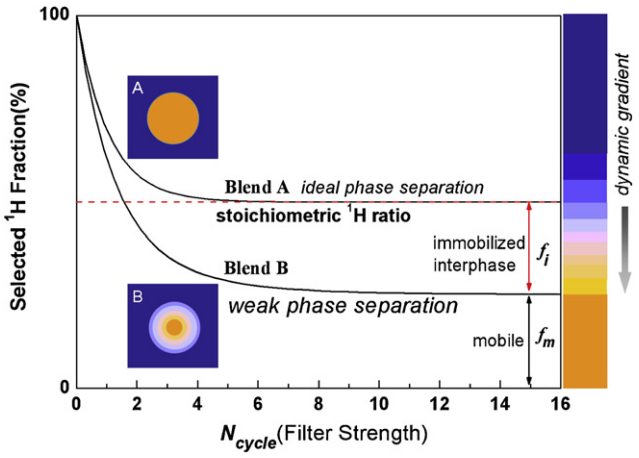

Fig. 15. Schematic curve of the selected fraction (end value) in spin diffusion experiment with increasing filter strength (N_{cycle}). The interphase, as well as the extent of phase separation in blends containing rigid and mobile domains can be determined from the curves.

Acknowledgments

This work was supported by National Natural Science Foundation of China (Grants 20774054, 20374031), the Joint-Research Foundation of the Nankai and Tianjin Universities by the Chinese Ministry of Education. We are grateful to Dr. X.L. Wang for his helpful discussions.

Appendix

Concerning the improvement of our previous NMR method to quantitatively determine the interphase thickness in multiphase polymers, we first briefly review the main features of the method proposed in our previous work [16]. Fig. 15 shows the schematic curves of the selected proton fraction (end value) in ^{1}H spin diffusion experiment with increasing filter strength (N_{cycle}) in two different polymer blends having weak (blend B) and ideal (blend A) phase separations, respectively. These two blends all contain a rigid (blue) and a mobile (orange) components, which are illustrated in Fig. 15, (for interpretation of the references to colour in this text, the reader is referred to the web version of this article) and the interphase with dynamic gradient is also illustrated. The most important significance of the curves in Fig. 15 is that the proton fraction of the interphase (f_i) can be directly determined from the difference of the stoichiometric proton ratio (dash line) of the dispersed phase (mobile component) with the final equilibrium value (f_m) of the selected mobile component at large N_{cycle}. On the basis of the measured interphase thickness, the extent of phase separation in polymer blends can be well evaluated.

Because the proton fraction of the interphase (f_i) and the mobile phase (f_m) can be quantitatively determined from the curves shown in Fig. 15, the interphase thickness (d_{itp}) for blend B in Fig. 15 can be directly estimated as the following formula on the basis of the geometrical relationship of the interphase and the dispersed phase [16]

$$d_{itp} = 0.5 \times \left(1 - \sqrt[p]{f_m/f_{sm}}\right) d_{dis} \quad (6)$$

where $f_{sm} = f_i + f_m$ represents the stoichiometric proton ratio of the dispersed phase (mobile component B including those in the interphase); p represents the dimension and its value depends on the

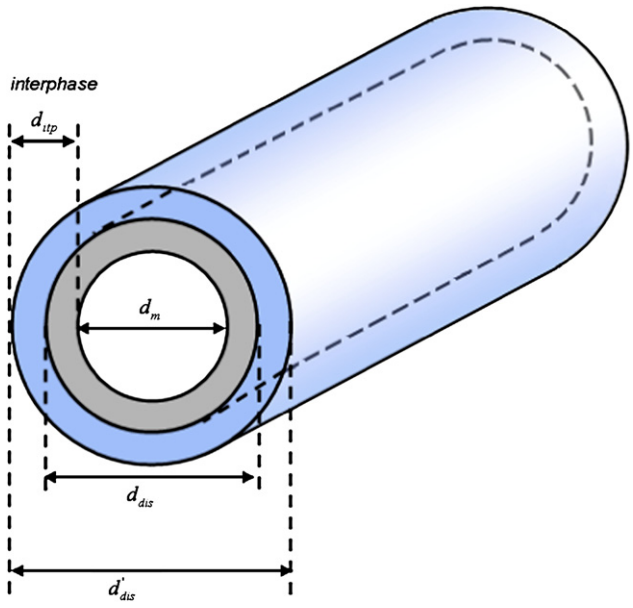

Fig. 16. Schematic diagram of the relationship of d_m, d_{dis}, d'_{dis} and d_{itp} for a cylindrical ($p = 2$) domain. Here, the length of the cylinder is considered to be far greater than d_{dis}. The contributions of both the rigid (blue) and the mobile (gray) components to the interphase are considered (for interpretation of the references to colour in this figure legend, the reader is referred to the web version of this article).

morphology: $p = 1$ for lamellar phase, 2 for cylinder with the length of the cylinder considered to be far greater than its diameter, and 3 for discrete phase, such as spheres in a matrix. It should be noted that only the immobilized component of the dispersed (mobile) phase (f_i) was considered to calculate the interphase thickness in Eq. (6). However, if we consider the intimate mixing and a continuous distribution of both the rigid and the mobile components in the interfacial region, the total proton fraction in the interphase region should be corrected to be $2f_i$ instead of f_i. Therefore, we can improve Eq. (6) to provide more accurate measurement of interphase thickness. Fig. 16 shows the schematic diagram of the improved geometrical relationship of d_{itp}, d_m, d_{dis} and d'_{dis} for $p = 2$ on the basis of the old model [16], where the dispersed phase d_{dis} corresponds to the diameter of dispersed phase having the stoichiometric ^{1}H ratio, and d'_{dis} denotes the diameter of the volume including total interphase region ($2f_i$) and the mobile phase (f_m). For easy comparison with the old model [16], the contribution of the rigid and the mobile components to the immobilized interphase was separately illustrated as blue and gray regions in Fig. 16, respectively, although they are actually mixed in interphase region.

On the basis of the geometry relationship obtained in our previous work [16] and improved model shown in Fig. 16, we can obtain the relationship between d_m and d_{dis}, as well as d_m and d'_{dis}:

$$d_m = \sqrt[p]{\frac{f_m}{f_i + f_m}}\, d_{dis} \tag{7}$$

$$d_m = \sqrt[p]{\frac{f_m}{2f_i + f_m}}\, d'_{dis} \tag{8}$$

It should be noted that the difference of the proton density of the two components was neglected in Eq. (8), and this condition is usually satisfied for most of the polymers. Thus the actual interphase thickness d_{itp}, including the two components at interphase region, should be written as:

$$\begin{aligned} d_{itp} &= (d'_{dis} - d_m)/2 \\ &= \left(1/\sqrt[p]{\frac{f_m}{2f_i + f_m}} - 1\right) \times d_m/2 \\ &= \left(1/\sqrt[p]{\frac{f_m}{2f_i + f_m}} - 1\right) \times \sqrt[p]{\frac{f_m}{f_i + f_m}} \times d_{dis}/2 \\ &= \left(\sqrt[p]{\frac{2f_i + f_m}{f_i + f_m}} - \sqrt[p]{\frac{f_m}{f_i + f_m}}\right) \times d_{dis}/2 \\ &= \left(\sqrt[p]{1 + \frac{f_i}{f_i + f_m}} - \sqrt[p]{1 - \frac{f_i}{f_i + f_m}}\right) \times d_{dis}/2 \\ &= \left(\sqrt[p]{1 + (f_i/f_{sm})} - \sqrt[p]{1 - (f_i/f_{sm})}\right) \times d_{dis}/2 \end{aligned} \tag{9}$$

Generally, we can directly obtain the selected fraction of the mobile phase (f_m) under strong dipolar filter strength. Therefore, it is convenient to calculate the interphase thickness from the following formula:

$$d_{itp} = \left(\sqrt[p]{2 - (f_m/f_{sm})} - \sqrt[p]{f_m/f_{sm}}\right) d_{dis}/2 \tag{10}$$

If we define a parameter $\lambda_{DFS} = f_m/f_{sm}$, then Eq. (10) can be written as:

$$d_{itp} = \left(\sqrt[p]{2 - \lambda_{DFS}} - \sqrt[p]{\lambda_{DFS}}\right) d_{dis}/2 \tag{11}$$

where λ_{DFS} can be directly measured from ^{1}H dipolar filter spin diffusion NMR experiments (see Fig. 15) and can be used to characterize the extent of the phase separation (see the following discussion).

On the basis of Eq. (11), the interphase thickness, d_{dis}, can be determined from the following two steps: (1) measuring λ_{DFS} by ^{1}H spin diffusion NMR experiments as shown in Fig. 15; (2) measuring d_{dis} by different techniques including NMR, TEM or SAXS etc. If d_{dis} can be measured by SAXS or TEM, then d_{itp} can be determined from Eq. (11). The advantage of this method is that it does not require the knowledge of the spin diffusion coefficients of the sample [28,49]. If SAXS and TEM cannot provide quantitative structural information due to either lower electron density contrast or low stain contrast between different phases (e.g. ER/EO80 in our previous work [16]), d_{dis} can be alternatively determined using the traditional initial slope approximation of the NMR spin diffusion curve as reported in previous literature [28], then d_{itp} can be directly obtained from Eq. (11). It should be mentioned here that Eq. (11) is a strict mathematical relationship between d_{itp} and d_{dis}, and has the advantage of avoiding any spin diffusion model and adjustable parameters which are needed in traditional NMR spin diffusion simulation. This is important for samples with extremely small interphase region, such as the case for UPR/EO80 in the present work. In principle, this method for measuring interphase thickness should be applicable to any multiphase polymers with detectable dynamic differences between different phases.

References

[1] Paul DR, Bucknall CB. Polymer blends: formulation and performance. New York: John Wiley and Sons; 2000.
[2] Araki T, Tran-Cong Q, Shibayama M. Structure and properties of multiphase polymeric materials. New York: Marcel Dekker; 1998.
[3] Lipic PM, Bates FS, Hillmyer MA. J Am Chem Soc 1998;120:8963–70.
[4] Hillmyer MA, Lipic PM, Hajduk DA, Almdal K, Bates FS. J Am Chem Soc 1997; 119:2749–50.
[5] Hadjichristidis N, Pispas S, Floudas G. Block copolymers: synthetic strategies, physical properties, and applications. New York: John Wiley and Sons; 2002.
[6] Grubbs RB, Dean JM, Broz ME, Bates FS. Macromolecules 2000;33:9522–34.

[7] Dean JM, Verghese NE, Pham HQ, Bates FS. Macromolecules 2003;36:9267–70.
[8] Mijovic J, Shen M, Sy JW, Mondragon I. Macromolecules 2000;33:5235–44.
[9] Guo Q, Thomann R, Gronski W. Macromolecules 2002;35:3133–44.
[10] Guo Q, Thomann R, Gronski W. Macromolecules 2003;36:3635–45.
[11] Guo Q, Harrats C, Groeninckx G, Koch MJH. Polymer 2001;42:4127–40.
[12] Xu ZG, Zheng SX. Macromolecules 2007;40:2548–58.
[13] Meng FL, Zheng SX, Li HQ, Liang Q, Liu TX. Macromolecules 2006;39:5072–80.
[14] Okada M, Fujimoto K, Nose T. Macromolecules 1995;28:1795–800.
[15] Pascault JP, Sautereau H, Verdu J, Williams RJJ. Thermosetting polymers. New York: Dekker; 2002.
[16] Sun PC, Dang QQ, Li BH, Chen TH, Wang YN, Lin H, et al. Macromolecules 2005; 38:5654–67.
[17] Sinturel C, Vayer M, Erre R, Amenitsch H. Macromolecules 2007;40:2532–8.
[18] Li XJ, Dang QQ, Lin H, Wang YN, Sun PC, Li BH, et al. Acta Polym Sin 2006;4: 636–9.
[19] Messori M, Toselli M, Pilati F, Tonelli C. Polymer 2001;42:9877–85.
[20] Zheng HF, Zheng SX, Guo QP. J Polym Sci Part A Polym Chem 1997;35:3161–8.
[21] Helfand E, Tagami Y. J Chem Phys 1972;56:3592–601.
[22] Helfand E, Sapse AM. J Chem Phys 1975;62:1327–31.
[23] Broseta D, Fredrickson GH, Helfand E, Leibler L. Macromolecules 1990;23:132–9.
[24] Liu RYF, Bernal-Lara TE, Hiltner A, Baer E. Macromolecules 2004;37:6972–9.
[25] Noro A, Okuda M, Odamaki F, Kawaguchi D, Torikai N, Takano A, et al. Macromolecules 2006;39:7654–61.
[26] Yeung C, Shi AC. Macromolecules 1999;32:3637–42.
[27] Lohse DJ, Russell TP, Sperling LH. Interfacial aspects of multicomponent polymer materials. New York: Plenum Press; 1997.
[28] Schmidt-Rohr K, Spiess HW. Multidimensional solid-state NMR and polymers. San Diego: Academic Press; 1994.
[29] Mirau PA. A practical guide to understanding the NMR of polymers. Wiley-Interscience Publisher; 2004.
[30] Kogler G, Mirau PA. Macromolecules 1992;25:598–604.
[31] Kao HM, Chao SW, Chang PC. Macromolecules 2006;39:1029–40.
[32] Li MJ, Chen Q. Polymer 2003;44:2793–8.
[33] Zhang LM, Tang HR, Hou GJ, Shen YD, Deng F. Polymer 2007;48:2928–38.
[34] Skogsberg U, Meyer C, Rehbein J, Fischer G, Schauff S, Welsch N, et al. Polymer 2007;48:229–38.
[35] Guo MM. Trends Polym Sci 1996;4:238–44.
[36] VanderHart DL, Asano A, Gilman JW. Chem Mater 2001;13:3781–96.
[37] Jia X, Wang XW, Tonelli AE, White JL. Macromolecules 2005;38:2775–80.
[38] Zhang L, Liu Z, Chen Q, Hansen EW. Macromolecules 2007;40:5411–9.
[39] Asano A, Tanaka C, Murata Y. Polymer 2007;48:3809–16.
[40] Zhang XQ, Do MD, Hoobin P, Burgar I. Polymer 2006;47:5888–96.
[41] Chaiyut N, Amornsakchai T, Kaji H, Horii F. Polymer 2006;47:2470–81.
[42] Landfester K, Spiess HW. Acta Polym 1998;49:451–61.
[43] Cai WZ, Schmidt-Rohr K, Egger N, Gerharz B, Spiess HW. Polymer 1993;34: 267–76.
[44] Wang XL, Tao FF, Sun PC, Zhou DS, Wang ZQ, Gu Q, et al. Macromolecules 2007;40:4736–9.
[45] Li BH, Xu L, Wu Q, Chen TH, Sun PC, Jin QH, et al. Macromolecules 2007;40: 5776–86.
[46] Kennedy SB, deAzevedo ER, Petka WA, Russell TP, Tirrell DA, Hong M. Macromolecules 2001;34:8675–85.
[47] Schmidt-Rohr K, Clauss J, Spiess HW. Macromolecules 1992;25:3273–7.
[48] Nagapudi K, Leisen J, Beckham HW, Gibson HW. Macromolecules 1999;32: 3025–33.
[49] Mellinger F, Wilhelm M, Spiess HW. Macromolecules 1999;32:4686–91.
[50] Mirau PA, Yang S. Chem Mater 2002;14:249–55.
[51] Wang J, Jack KS, Natansohn AL. J Chem Phys 1997;107:1016–20.
[52] Clauss J, Schmidt-Rohr K, Spiess HW. Acta Polym 1993;44:1–17.
[53] VanderHart DL, McFadden GB. Solid State Nucl Magn Reson 1996;7:45–66.
[54] Demco DE, Johanson A, Tegenfeldt J. Solid State Nucl Magn Reson 1995;4:13–38.
[55] Buda A, Demco DE, Bertmer M, Blulmich B, Litvinov VM, Penning JP. J Phys Chem B 2003;107:5357–70.
[56] Brus J, Dybal J, Schmidt P, Kratochvil J, Baldrian J. Macromolecules 2000;33: 6448–59.
[57] Clayden NJ, Nijs CL, Eeckhaut GJ. Polymer 1997;38:1011–6.
[58] Buda A, Demco DE, Blumich B, Litvinov VM, Penning JP. ChemPhysChem 2004; 5:876–83.
[59] Tambasco M, Lipson JEG, Higgins JS. Macromolecules 2006;39:4860–8.
[60] Horng TJ, Woo EM. Polymer 1998;39:4115–22.
[61] Nishi T, Wang TT. Macromolecules 1975;8:909–15.
[62] Fukada T, Nagata M, Inagaki H. Macromolecules 1984;17:548–53.
[63] Kalogeras IM, Stathopoulos A, Vassilikou-Dova A, Brostow W. J Phys Chem B 2007;111:2774–82.